

**Thiol Functionalized and Manganese Dioxide  
Doped Biochar for the Removal of  
Toxic Organic and Inorganic Contaminants  
from Water**

Eshani Jha  
Lynbrook High School, San Jose, CA

## I. Abstract

Less than one percent of the earth’s water is easily accessible to us as freshwater and nearly half of this water is heavily polluted with pesticides, emerging contaminants, and heavy metals due to waste from industry, human establishments, and agriculture. This research aimed to remove these key classes of contaminants by manipulating biochar surface area, controlling chemical composition and catalytic properties for oxidative breakdown, adding surface complexing agents, and modifying intrinsic pore size. Six different kinds of engineered biochar were placed in water with 100µM initial pp-DDT, pp-DDE, dimetridazole, bisphenol-A, arsenic, lead, mercury, and cadmium concentrations. Results indicate that catalyst and surface complexing agent presence coupled with high surface area are key for contaminant removal: manganese oxide and thiol functionalized milled rice husk biochar removed over 94% pesticides, 53% pharmaceuticals, 95% microplastics, and 96% heavy metals within 10 minutes. Integrating engineering with environmental chemistry, an effective filter with a cost of less than \$1 per month and a filtration rate exceeding that of commercial filters can be created for global distribution and use.

## II. Acknowledgements

Professor Bhoopesh Mishra at the Illinois Institute of Technology and Dr. Felix Grun at the University of California, Irvine helped me understand complex concepts, mitigated experimental error, and provided me with well-equipped laboratories for my research. Dr. Krista Hennig at the Pasca Lab of Stanford University deepened my understanding of arsenic neurotoxicity by providing access to extensive literature. Dr. James Carthew at the Greenfield Labs of Ford Motor Company established an industrial partnership with me to test factory waste water and mass produce my filter. Mr. Isaac Pallone, my teacher at Lynbrook High School, refined my research goals and kept track of my progress for timely completion.

## III. Biography

Eshani Jha is a senior at Lynbrook High School in San Jose, California. She first became interested in research in 7<sup>th</sup> grade through her school’s science fair and has been conducting research on water purification for the past five years.

Eshani was an oral presenter at the American Chemical Society Fall 2020 Virtual Meeting & Expo and the 2020 International Conference on Environmental Engineering and Materials Science. She will be presenting her research at the Asia Oceania Geosciences 2021 Virtual Meeting. She has also won many awards for her work and was named a Top Winner (3<sup>rd</sup> Place) at the Regeneron Science Talent Search, a 2019 and 2021 National Junior Science and Humanities Symposium National Participant and State Winner, and a 2019 GENIUS Olympiad International finalist.

Outside of the lab, Eshani enjoys singing and playing the sitar. She is a published author and her book, *Legal Status*, was named an Amazon bestseller. At her school, she is an officer of the National Spanish Honor Society and a Legislative Council representative. Ultimately, she hopes to contribute to the development of our society through research and innovation.

## IV. Table of Contents

1.0	Introduction .....	2
2.0	Background.....	3
3.0	Project Progression.....	4
4.0	Materials and Methods .....	6
5.0	Results and Discussion .....	10
6.0	Engineering Application.....	16
7.0	Conclusion and Expected Impact .....	18
8.0	References .....	19

## 1.0 Introduction

Water potability remains a key challenge of modern civilization. Worldwide, over two billion people lack access to clean water and at least 80% of the world's wastewater is dumped back into the environment without proper treatment, polluting rivers, lakes, and oceans [1, 2]. Meanwhile, our freshwater sources are finite: less than 1% of the earth's water is easily accessible to us through rivers, lakes, and streams and nearly half of this water is heavily polluted [3].

The Agency for Toxic Substances and Disease Registry releases a Substance Priority List biannually to address this issue of water contamination, ranking contaminants in order of their toxicity and potential for exposure. According to this list, three classes of contaminants are of primary concern: organochlorine pesticides such as pp-DDT and pp-DDE (a metabolite of pp-DDT), emerging contaminants such as dimetridazole (a pharmaceutical) and bisphenol A (a microplastic), and heavy metals such as arsenic, lead, mercury, and cadmium.

### 1.1 Pesticides

Pesticides are commonly used to protect crops and play a significant role in food production. However, only 5% of sprayed herbicides and 2% of sprayed insecticides reach their intended destinations or target species [4, 5]. The remaining pesticides are transported via runoff and wind to aquatic environments, grazing areas, and human settlements [6]. Of special concern are organochlorine pesticides, which have long half-lives that allow them to persist in the environment decades after initial exposure [6].

pp-DDT, an organochlorine insecticide, was commonly used to control infectious disease vectors, such as mosquitoes [7]. Because it has a half-life of 150 years, even though it was discontinued two decades ago, it remains prevalent in aquatic environments, thereby acting as a sink for long-term exposure. pp-DDT degrades to form pp-DDE. pp-DDT and pp-DDE are then readily taken up by organisms from surrounding media and food due to its high lipid solubility, which allows for retention in fatty tissue and subsequent biomagnification along the food chain [8]. One effect of exposure is hyperplasia, which is the enlargement of organs or tissues due to increased reproduction rates of cells. This leads to tumor formation (cancer). pp-DDT and pp-DDE are also endocrine disruptors that activate estrogen receptors and inhibit androgen receptors, leading to over and under expression of key genes. On the Substance Priority List, pp-DDT is ranked 15<sup>th</sup> while pp-DDE is ranked 21<sup>st</sup> [4].

### 1.2 Emerging Contaminants

Recently, a new class of contaminants called "Emerging Contaminants" has become increasingly common. Despite having significant ecological and human health impacts, they remain unregulated under current environmental laws and hence untreated in drinking and waste water [9]. Moreover, sequestration technologies such as reverse osmosis and water acidification are largely ineffective for remediation.

A major class of emerging contaminants is pharmaceuticals. Since they are not completely absorbed by living systems, they are commonly found in sewage water, which ultimately merges with freshwater bodies [10, 11]. Dimetridazole, an antiprotozoal drug, is used for animal and livestock treatment. However, 40–90% of the ingested amount is excreted [12]. Since the antibiotic remains active after excretion, it gives rise to resistant bacterial strains. In one study, bacterial populations from water near large farms were five times as resistant to antibiotics as normal microbial strains [13].

Another major class of emerging contaminants is microplastics, such as BPA (bisphenol A). BPA is often used in containers (e.g. water bottles), but it can break off from the containers as microplastic and seep into food or beverages [14]. For instance, a study that had people eat one serving of soup found that urine levels of BPA were 1,221% higher in those who consumed canned soup compared to those who consumed fresh soup. Additionally, WHO reported that BPA levels in breastfed babies were up to eight times lower than those in babies fed liquid formula from BPA-containing bottles [15]. BPA is a known carcinogen.

### 1.3 Heavy Metals

Due to their widespread applications, heavy metals have established a ubiquitous presence in the environment. Concerns regarding their detrimental effects on humans and the ecosystem are not issues to be

associated only with developing countries (e.g. Bangladesh), but also highly developed countries such as the US itself (e.g. Flint, MI lead poisoning). On the Substance Priority List, arsenic ranks 1<sup>st</sup>, lead ranks 2<sup>nd</sup>, mercury ranks 3<sup>rd</sup> and cadmium ranks 7<sup>th</sup> [4].

Arsenic is a ubiquitous element that is detected at low concentrations in virtually all environmental matrices [16]. Environmental pollution by arsenic occurs both as a result of natural phenomena and industrial manufacturing. Worldwide, at least 140 million people in 50 countries drink water with arsenic concentrations exceeding 10 ppb. The EPA guideline is 0 ppb for human consumption.

Lead occurs naturally in the environment, but anthropogenic activities contribute to the release of high concentrations [17]. Lead poisoning directly results in at least 412,000 deaths per annum in just the US [18]. On the global scale, each dollar invested towards lead contamination prevention can result in a net savings of \$181-\$269 billion, which is a cost-benefit ratio exceeding that of even vaccines [19].

Mercury is a liquid metal at ambient temperatures and pressures. There are multiple EPA superfund sites for mercury in the US (**Fig. 1**). The EPA recently adopted its first ever mercury toxicity rule, and it is estimated that this rule will prevent, annually, up to 6,000 heart attacks, 130,000 asthma attacks, and 4,000-11,000 premature deaths as well as save \$40-\$70 billion in healthcare costs in the US alone [18].

Cadmium is widely distributed in the earth's crust and is frequently used in various industrial activities [22]. Human exposure to cadmium occurs through ingestion of contaminated food or water [23]. Cadmium is also a highly toxic and prevalent heavy metal, with at least 5 million people at risk for exposure to cadmium globally, with an estimated disease burden of 250,000 disability-adjusted life years.

All four heavy metals are carcinogenic and poisoning effects (e.g. Minamata disease for mercury, itai-itai disease for cadmium) are irreversible.

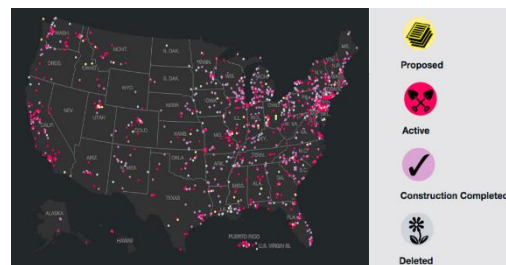


**Figure 1** EPA Superfund sites across US.

## 2.0 Background

Current water filters commonly use activated carbon. Activated carbon effectively removes chemicals such as chlorine and volatile organic compounds such as benzene from water [24]. However, it does not successfully filter organochlorines, emerging contaminants, or heavy metals. Hence, the goal of this research was to design efficient, sustainable, and affordable filtration material for the rapid removal of these contaminants from water.

### 2.1 Biochar

Biochar is often confused with activated carbon, a generic term loosely used for carbonaceous materials that have undergone some form of physical or chemical activation. For example, a coconut husk passed through steam is an activated carbon. Within the activated carbon family, there are two class of well-defined chemical processes: pyrolysis and hydrothermal carbonization [25]. Pyrolyzed carbon, or biochar, is produced by the chemical breakdown of carbonaceous feedstocks under high temperatures (typically between 450°C and 850°C) in an inert atmosphere [26]. Biochar can also be physically or chemically activated using acids, steam, gases, and/or metals. Biochar is composed of carbon matrices, giving it a chemically stable honeycomb-like structure and providing a perfect substrate for physical and chemical modifications [27]. Biochar can be synthesized from biowaste (e.g. rice husk, spent coffee ground) and simultaneously retain the functional groups and properties of the initial feedstock, which makes biochar extremely well suited for use in contaminant sequestration [28, 29].

### 2.2 Functionalization of Biochars

Functionalized biochars resulting from the addition of dopants (e.g. minerals and inorganics) to the carbon matrix demonstrate a dramatic enhancement in the rate and extent of contaminant uptake [30]. Through manipulation of synthesis conditions, this can also lead to increased selectivity for certain pollutants. Thus, biochar has immense potential for sustainable remediation in complex systems.

This research explored the effects of three chemical dopants on contaminant uptake: manganese oxide ( $\text{MnO}_2$ ), zinc oxide ( $\text{ZnO}$ ), and thiol (SH). Manganese oxide is one of the best natural scavengers of contaminants and controls the distribution and bioavailability of many organic and inorganic compounds through oxidative redox transformations [31]. Zinc oxide has been shown to decrease the average pore spacing of biochar by collapsing macropores [32]. Thiols are known to be strong complexing agents for a variety of organic and inorganic pollutants [33]. Given these properties, functionalized biochar is expected to remediate water with all three classes of contaminants discussed.

### 3.0 Project Progression

I have been conducting research on contaminant sequestration for the past four years. My research has been divided into 3 phases: natural organic matter for mercury sequestration, functionalized nanoparticles for heavy metal removal, and functionalized biochar for inorganic and organic contaminant removal (current year).

#### 3.1 Natural Organic Matter

My first year of research, I explored the stabilization mechanism of mercury sulfide minerals in lakes and other aquatic systems. I hypothesized that Natural Organic Matter (NOM) coating on the surface of mercury minerals would inhibit their conversion to ionic (highly toxic) mercury.

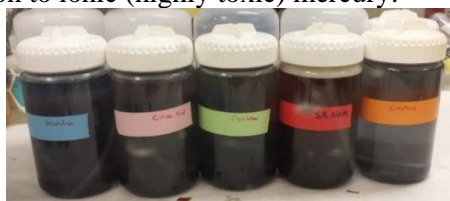


**Fig. 2** (From left to right) Histidine, citric acid, cysteine, and SR-NOM in Teflon flask with metacinnabar. (R) Control flask (no NOM in flask).

(Picture taken by: Eshani Jha)

To test my hypothesis, I added a constant amount of metacinnabar to 10 Teflon bottles for concentrations of 10ppm. To simulate the natural condition of aquatic systems due to decaying matter and other biological substances, I also added a constant amount of cysteine (sulfur-containing ligand), histidine (nitrogen-containing ligand), citric acid (oxygen-containing ligand), and SR-NOM (sulfur, nitrogen, and oxygen) (**Fig. 2**). After 2 weeks, I filtered out the NOMs and measured their weights to determine amount of mercury bound to them. Among the NOMs studied, cysteine was the most effective inhibitor of mercury dissolution at only 5.64% metacinnabar dissolved after 2 weeks. Hence, cysteine forms very strong, long-lasting bonds with Hg and is an opportune candidate for inhibiting the pool of ionic mercury in water via dissolution of mineralized mercury.

#### 3.2 Functionalized Nanoparticles (Year 2)

My next two years, I explored the use of thiol groups, which are characteristic of cysteine, for removal of heavy metals from water. I created a water filter using thiol-functionalized silica nanoparticles (thiol chemically bonded to silica nanoparticles) to remove cadmium and mercury (Phase I) as well as arsenic and lead (Phase II) from water.

I constructed my filter by first cutting holes in microcentrifuge tubes to construct “windows” and then covering the windows with filter paper. To allow for local and remote monitoring of the filtration process, I connected a LightBlue Bean and an Arduino sensor to my filter. I placed my filter in contaminated water with heavy metal concentrations of 10ppm for 15 minutes, 30 minutes, and 120 minutes, and 2 days (**Fig. 3**).

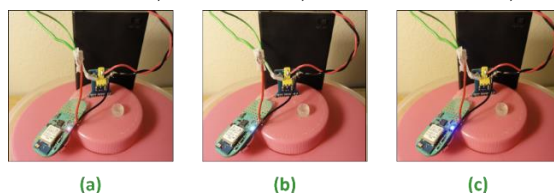


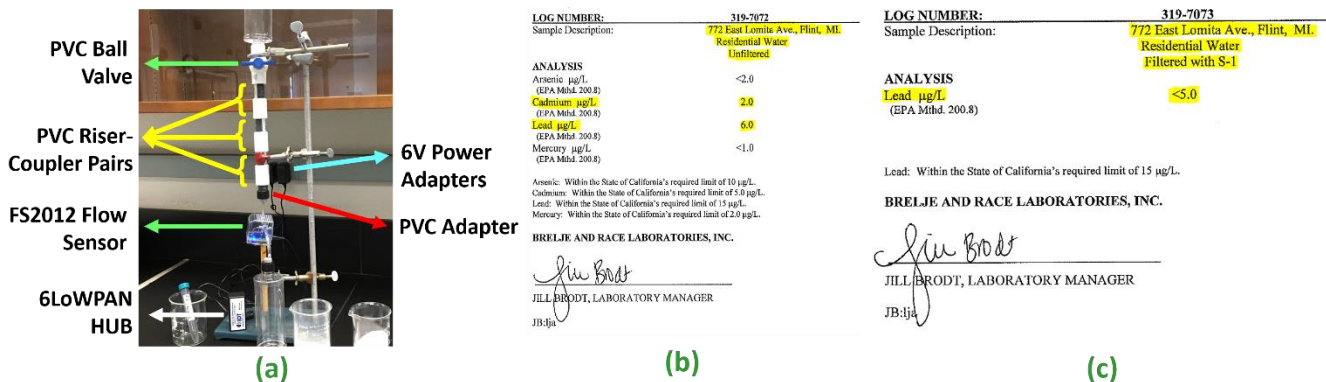
**Fig. 3** Filtration setup with LED on LightBlue Bean turning a) red in 15 mins, b) green in 30 mins, and c) blue in 120 mins.

(Picture taken by: Eshani Jha)

After the filtration process, I used Inductively Coupled Plasma Mass Spectrometry (ICP-MS) to measure remaining heavy metal concentrations (to 1ppb). My filter demonstrated complete removal of lead, mercury, and cadmium for all data points.

### 3.3 Thiol Functionalized Biochar (Year 3)

Last year, I tested the filtration ability of thiol-functionalized biochar. I engineered a filter using sand, calcite, and enhanced biochar (Fig. 4a). Filter effectiveness was measured by passing contaminated water through the filter at flow rates of 15mL/min, 30mL/min, and 120mL/min. Results of ICP-MS Analysis indicated all contaminants were removed for 15mL/min and 30mL/min filtration rates.



I also tested my filter with water from Flint, MI (Fig. 4b and 4c). Results were certified by Brejle and Race Labs, an EPA-approved lab in Santa Rosa, CA. Unfiltered river water obtained from Flint, MI residents lead concentrations of 6.0ppm and cadmium concentrations of 2.0ppm. After filtration using functionalized nanoparticles, the concentration of lead was undetectable.

### 3.4 Functionalized Biochar: Experimental Design (Current Year)

Experimentation was divided into 3 phases: Phase I (biochar engineering and functionalization), Phase II (pesticide and emerging contaminant testing), and Phase III (heavy metal testing).

In Phase I, six kinds of biochar were engineered with different properties to maximize contaminant uptake. Specifically, a) surface area, b) catalyst presence, c) pore size, d) surface complexing agent presence, and e) and carbon composition were manipulated to enhance contaminant removal.

- To determine the effect of surface area on sequestration efficiency, MnO<sub>2</sub>-SH doped milled rice husk biochar was compared to MnO<sub>2</sub>-SH doped (unmilled) rice husk biochar. Here, milling was the dependent variable.
- To determine the effect of catalyst presence on sequestration efficiency, MnO<sub>2</sub>-SH doped rice husk biochar was compared to SH doped rice husk biochar. Here, MnO<sub>2</sub> presence was the dependent variable.
- To determine the effect of pore size on sequestration efficiency, ZnO-SH doped rice husk biochar was compared to SH doped rice husk biochar. Here, ZnO presence was the dependent variable.
- To determine the effect of surface complexing agent presence on sequestration efficiency, SH doped rice husk biochar was compared to undoped rice husk biochar. Here, SH presence was the dependent variable.
- To determine the effect of carbon composition on sequestration efficiency, undoped rice husk biochar was compared to undoped oak wood biochar. Here, initial feedstock was the dependent variable.

Thus, a total of six different kinds of biochar were produced: (i) MnO<sub>2</sub>-SH doped milled rice husk biochar (RHB), (ii) MnO<sub>2</sub>-SH doped unmilled RHB, (iii) ZnO-SH doped RHB, (iv) SH doped RHB, (v) undoped RHB, and (vi) undoped oak wood biochar (OWB) (Fig. 5). XANES spectra were used to ascertain that functionalization of biochars with MnO<sub>2</sub>, ZnO, and SH was successful.

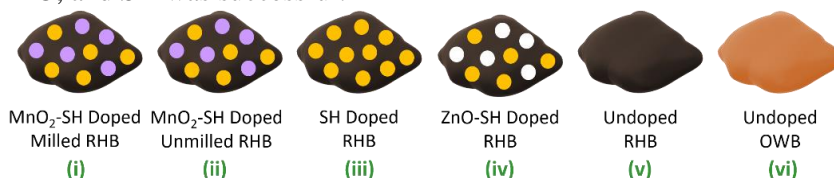


**Figure 5** Six types of biochar tested. Purple dots represent MnO<sub>2</sub> dopant, yellow dots represent SH dopant, white dots represent ZnO dopant, dark brown represents RHB, and light brown represents OWB.

*Notes: Figure not to scale or color, all types of biochar appear black in real life.*

*(Image created by: Eshani Jha)*

In Phase II, the ability of the various types of biochar to sequester organic contaminants was tested. The six kinds of biochar were each placed in water contaminated with pesticides (pp-DDT and pp-DDE) and emerging contaminants (BPA and dimetridazole). Gas chromatography mass spectrometry (GC-MS) was used to determine final contaminant concentrations in the filtrate solutions.

In Phase III, the ability of the various types of biochar to sequester inorganic contaminants was tested. The six kinds of biochar were each placed in water contaminated with arsenic, lead, mercury, and cadmium. Inductively coupled plasma mass spectrometry (ICP-MS) was used to determine final contaminant concentrations in the filtrate solutions. An overview of Phase II and Phase III is given (Fig. 6).

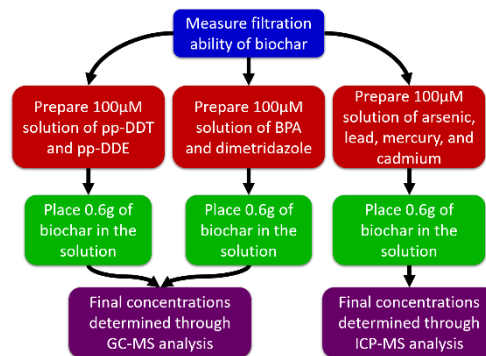


**Figure 6** Overview of Phase II and Phase III.

*(Image created by: Eshani Jha)*

## 4.0 Materials and Methods

### 4.1 Phase I – Biochar Production and Functionalization

First, 50g of rice husks were obtained for RHB and 10g of oak wood was obtained for oak wood biochar (OWB). For undoped RBH, 10g of rice husks were set aside. Rice husks for doped RHB (40g) were split into four categories with 10g each: MnO<sub>2</sub>-SH doped milled, MnO<sub>2</sub>-SH doped unmilled, ZnO-SH doped, and SH doped.

The rice husks for MnO<sub>2</sub> doping (20g) were first submerged in a 1L 200mM solution of MnCl<sub>2</sub>. After 20 hours, husks were filtered from the solution using a filtration syringe and 0.65µm filter paper. They were then submerged in a boiling 1L solution of 200mM KMnO<sub>4</sub> for 4 hours. The husks were filtered from the solution using a filtration syringe and 0.65µm filter paper.

The rice husks for zinc oxide doping (10g) were submerged in a 1L 200mM solution of Na(CO<sub>3</sub>)<sub>2</sub> for 20 hours. The solution was then electrolyzed with a zinc anode for 4 hours. The husks were filtered from the solution using a filtration syringe and 0.65µm filter paper.

Then, four separate 200mM solutions of cysteine (to avoid cross-contamination) were prepared and all rice husks for doping (40g) were submerged in separate solutions for 24 hours. Cysteine is an amino acid with a thiol side change and thus serve as the thiol-containing ligand for functionalization of biochar.

Pyrolysis was separately carried out on each type of biomass (total 60g: 10g undoped RHB, 40g doped RHB, and 10g undoped OWB) using a vertical tube furnace at temperatures of 450°C under a 20mL/min flow of nitrogen gas for 2 hours to achieve high effective surface area (Fig. 7). Biochar was heated in an oven at 80°C for 3 days. A summary is given below (Fig. 8).

To establish that β-MnO<sub>2</sub> (the most reactive form of MnO<sub>2</sub>) was the dominant phase of in MnO<sub>2</sub>-SH doped RHB and that functionalization of MnO<sub>2</sub> was successful, Manganese K-edge XANES was conducted. To establish that ZnO functionalization and SH functionalization were successful, Zinc K-edge XANES and Sulfur K-edge XANES were also conducted.

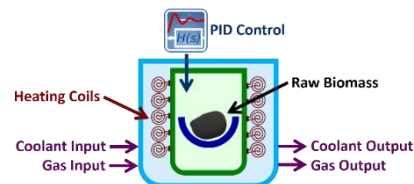


**Figure 7** Schematic of vertical furnace tube for biochar pyrolysis.

*(Image created by: Eshani Jha)*

The biochars were placed in centrifugal vials (all biochars were kept in separate vials to avoid cross-contamination). The biochars were equilibrated for 24 hours in a mildly acidic buffer (pH  $5.5 \pm 0.2$ ) to bring the pH of the biochars to a neutral pH range (biochar is naturally alkaline due to the enrichment of alkaline earth metals and removal of acidic functional groups during pyrolysis).



**Figure 8** Summary of biochar production process.  
(Image created by: Eshani Jha)

Half of the  $\text{MnO}_2$ -SH doped biochar was then milled using a mortar and pestle while the other half remained un-milled, creating  $\text{MnO}_2$ -SH doped milled RHB and  $\text{MnO}_2$ -SH doped unmilled RHB. Thus, a total of six different biochar samples were created: (i)  $\text{MnO}_2$ -SH doped milled RHB, (ii)  $\text{MnO}_2$ -SH doped unmilled RHB, (iii) ZnO-SH doped RHB, (iv) SH doped RHB, (v) undoped RHB, and (vi) undoped OWB (**Fig. 5**).

#### 4.2 Phase I – XANES Analysis

Ascertaining the phase of the nano-materials ( $\text{ZnO}$  and  $\text{MnO}_2$ ) and species of the organic ligand (thiol) functionalized on the biochar was essential for desired properties of the biochar. XANES, which is a powerful technique for probing oxidation state and ligation environment of the element under probe, was used for this purpose. Sulfur K-edge XANES spectra, Zinc K-edge XANES spectra, and Manganese K-edge XANES spectra for standard complex samples and doped biochar samples were acquired at the Advanced Photon Source (Argonne National Lab, Lemont, IL) on beamline 13-ID-E in fluorescence detection mode.

At 13-ID-E, signal from higher order harmonics was removed by detuning the monochromator to fifty percent of the maximum beam flux and peaks were normalized through energy calibrations. XANES measurements were conducted from 2460-2500eV for sulfur, 9650-9750eV for zinc, and 6530-6830eV for manganese. For sulfur, step sizes in the near-edge regions (2464-2484eV) were 0.1eV. For zinc and manganese, step sizes in the near edge-regions (9650-9675eV and 6540-6570eV, respectively) were 0.5 eV respectively. In pre-edge and post-edge regions, step sizes were 0.2eV for sulfur and 1.0 eV for zinc and manganese. Results are shown in **Section 5.1, 5.2, and 5.3**.

#### 4.3 Phase II – Biochar Testing for Pesticide and Emerging Contaminant Removal

A total of 0.6g of each type of the six types biochar was placed in six different centrifuge vials (0.05g per vial). The vials were then filled to the 10mL mark with methanol. The vials were centrifuged at 4000rpm for 5 minutes. Supernatant methanol (~8mL) was pipetted out and discarded. The vials were then filled to the 10mL mark with distilled water. The vials were again centrifuged at 4000rpm for 5 minutes. Supernatant distilled water (~8mL) was pipetted out and discarded.

From each vial, 1mL of the solutions were pipetted into separate microcentrifuge vials labeled according to biochar type. To each vial, 1mL dichloromethane (DCM) was added. The vials were vortexed and 0.5mL of the DCM solution (bottom layer) was pipetted out (these solutions served as the matrix for GC-MS analysis). The remaining solutions from the DCM vials and the remaining supernatant solutions from the biochar vials (~7mL) were pipetted out and discarded.

In each biochar vial, 10mL of stock solution was added. This stock solution contained 100 $\mu\text{M}$  concentrations of pp-DDE, pp-DDT, dimetridazole, and bisphenol A. The vials were then briefly shaken and allowed to settle for 10 minutes.

After 10 minutes, the vials were again shaken for solution homogenization before pipetting 2mL from each vial into separate microcentrifuge vials. These vials were centrifuged at 13200rpm for 7 minutes. The supernatant from these vials (~1.5mL) were pipetted into different microcentrifuge vials and once again centrifuged at 13200rpm for 7 minutes.

Then, 1mL from each vial was pipetted into a different microcentrifuge vial, to which 0.5mL DCM was added. The vials were vortexed and 0.25mL of the DCM solution (bottom layer) was pipetted out. This filtrate was analyzed using GC-MS analysis.

The procedure was repeated a total of three times for three trials. Additionally, each solution was analyzed three times to mitigate machine error.

#### 4.4 Phase II – GC-MS Analysis

Final pesticide, pharmaceutical, and microplastic concentrations were analyzed using GC-MS Analysis. GC-MS instruments separate chemical mixtures and identify components at a molecular level. The instrument operates on the principle that a mixture will separate into individual substances when heated. Compounds are identified by comparing analyte mass and spectra against a library of known mass spectra. GC-MS spectra were acquired at the University of California, Irvine using a ThermoFinnegan TraceMS+ System. The machine was run in positive EI mode. To determine final contaminant concentrations, calibration curves were generated. Stock solutions of each contaminant with concentrations of 100 $\mu$ M, 33 $\mu$ M, 11 $\mu$ M, 3 $\mu$ M, and 1 $\mu$ M were analyzed (**Fig. 10a**). The area under the peaks was calculated using Chromeleon Chromatography Data System Software. These areas were used to derive a calibration curve, with concentration expressed as a linear function of area using Least Squares Regression (**Fig. 10b**). Matrix solutions (effluent from biochar prewash) were analyzed and resulting spectra were used to determine pre-existent compounds and corresponding spectra. In the resulting spectra obtained from GC-MS, spikes occurred at various locations along both the filtrate solutions and the matrix solutions (**Fig. 11**). These spikes represent alkane chains from the biochar and were a result of the initial feedstock.

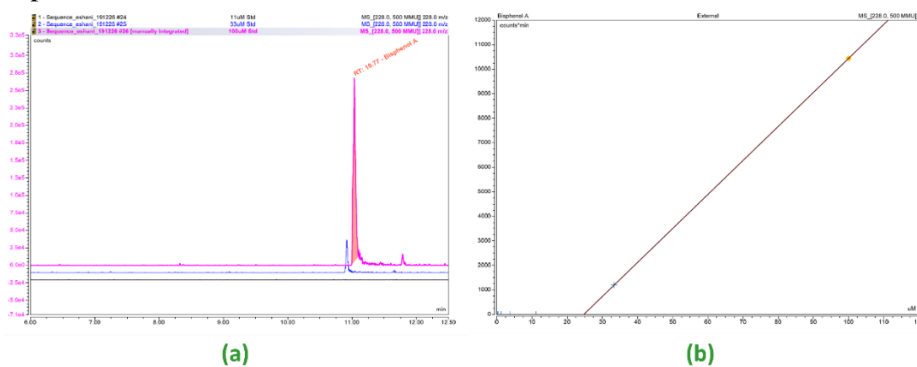


**Fig. 10** (a) Chromatogram for GC-MS BPA calibration; (b) the calibration curve for BPA. Chromatograms and calibration curves were obtained for all contaminants.

*(Image obtained from: University of California, Irvine, CA)*

In OWB, many scattered larger peaks can be found in the chromatograms (**Fig. 11a**). These peaks correspond to short, reactive alkanes commonly found in lignin, a component of wood. The smaller, sparser peaks detected in rice husk biochar represent long chain alkanes common in plant leaves and cuticles (**Fig. 11b**).

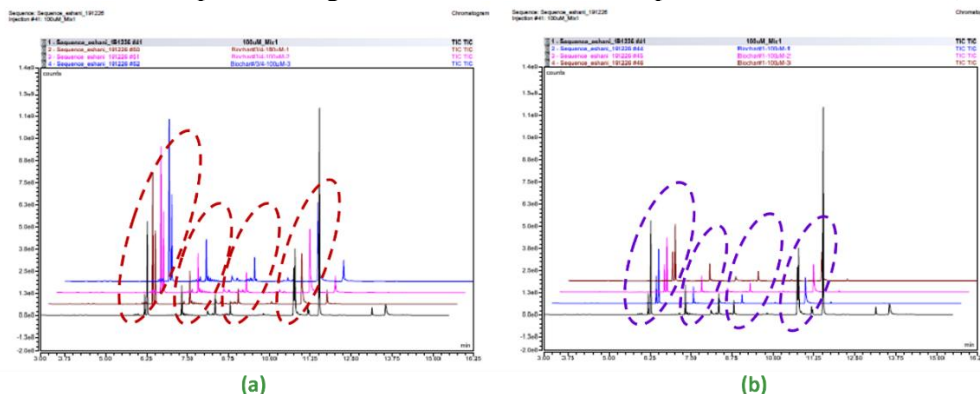


**Fig. 11** (a) Chromatograms for OWB GC-MS matrix; (b) Chromatograms for RHB ICP-MS matrix.

*(Image obtained from: University of California, Irvine, CA)*

The areas under peaks of the filtrate solutions were then substituted into the respective calibration curves to obtain final contaminant concentrations in the filtrate solutions. The percent of contaminant sequestered was calculated using the formula:

$$\text{Percent removed} = \left(1 - \frac{\text{Filtrate Concentration}}{\text{Initial Concentration of } 100\mu\text{M}}\right) \times 100$$

216 chromatograms were obtained and analyzed for filtrate solutions:

$$6 \text{ types of biochar} \times \frac{3 \text{ trials}}{\text{contaminant}} \times \frac{3 \text{ readings}}{\text{trial}} \times 4 \text{ contaminants} = 216 \text{ chromatograms}$$

72 chromatograms were obtained and analyzed for stock solutions for calibration curves:

$$6 \text{ stock solutions} \times \frac{3 \text{ readings}}{\text{solution}} \times 4 \text{ contaminants} = 72 \text{ chromatograms}$$

Thus, a total of 288 chromatograms were obtained and analyzed for GC-MS. Results are shown in **Section 5.4, 5.5, and 5.6.**

#### 4.5 Phase III – Biochar Testing for Heavy Metal Removal

A total of 0.3g of each type of the six types biochar was placed in six different centrifuge vials (0.05g per vial). The vials were then filled to the 10mL mark with methanol. The vials were centrifuged at 4000rpm for 5 minutes. Supernatant methanol (~8mL) was pipetted out and discarded. The vials were then filled to the 10mL mark with distilled water. The vials were again centrifuged at 4000rpm for 5 minutes. Supernatant distilled water (~8mL) was pipetted out and discarded.

To each biochar vial, 10mL of stock solution was added. This stock solution contained 100 $\mu$ M concentrations of potassium arsenate, lead (II) chloride, mercury (II) chloride, and cadmium (II) chloride. The vials were then briefly shaken and allowed to settle for 15 minutes.

After 15 minutes, the vials were again shaken for solution homogenization before pipetting 2mL from each of them into separate microcentrifuge vials. These vials were centrifuged at 13200rpm for 7 minutes. Supernatant (~1.5mL) was pipetted out from each vial into a different microcentrifuge vial and once again centrifuged at 13200rpm for 7 minutes. Then, 1mL was pipetted from each vial into a different microcentrifuge vial, to which 0.5mL 3M hydrochloric acid was added. These vials were shaken and 0.25mL of each solution was pipetted out. This solution was analyzed through ICP-MS analysis.

The procedure was repeated a total of three times for three trials. Additionally, each solution was analyzed three times to mitigate machine error.

#### 4.6 Phase III – ICP-MS Analysis

Final heavy metal concentrations were analyzed using ICP-MS Analysis. ICP-MS instruments analyze elements through ion generation. By passing the sample through a high-temperature (~10,000°C) plasma source, atoms are ionized and then sorted according to their mass/charge ratio (m/z). An electron multiplier tube detector then identifies and quantifies each ion.

ICP-MS spectra were acquired at the Illinois Institute of Technology, Chicago, IL using a Perkin-Elmer Elan DRC ICP-MS System. To determine final contaminant concentrations, spectra were analyzed using the methods detailed in **Section 4.4.**

216 samples were obtained and analyzed for filtrate solutions:

$$6 \text{ types of biochar} \times \frac{3 \text{ trials}}{\text{contaminant}} \times \frac{3 \text{ readings}}{\text{trial}} \times 4 \text{ contaminants} = 216 \text{ samples}$$

72 samples were obtained and analyzed for stock solutions for calibration curves:

$$6 \text{ stock solutions} \times \frac{3 \text{ readings}}{\text{solution}} \times 4 \text{ contaminants} = 72 \text{ samples}$$

Thus, a total of 288 samples were obtained and analyzed for ICP-MS. Results are shown in **Section 5.7.**

#### 4.7 Statistical Significance of Results

All data groups for each contaminant type were tested to determine the difference ( $d_0$ ) between the data means using two-sample t-tests. In all tests, the null hypothesis was that the sample means, or the percent of that contaminant removed by two types of biochar, were equal ( $H_0: \mu_1 = \mu_2$ ). The alternate hypothesis was that the sample means, or the percent of that contaminant removed by two types of biochar, were not equal ( $H_A: \mu_1 \neq \mu_2$ ). The test statistic  $t$  was computed using the formula:

$$t = \frac{[(x_1 - x_2) - d]}{\sqrt{\frac{s_1^2}{n_1} + \frac{s_2^2}{n_2}}}$$

Where  $x$  was the mean of the sample,  $d$  was the hypothesized difference between the population means,  $s$  was the standard deviation of the sample, and  $n$  was the size of the sample. Since the sample sizes were equal, the degrees of freedom were approximated to  $n - 1$ . Then, the  $p$  - value, or the probability of observing a sample statistic as extreme as the test statistic  $t$ , was assessed using a  $t$  - Distribution Chart and the computed  $t$  value and degrees of freedom.

The significance level was calculated as  $100 - p$ . The null hypothesis ( $H_0$ ) was rejected when the significance level was greater than 95%. This implied that data groups were significantly different from each other at least at the 95% confidence level.

Thus, differences between percent contaminant removed by different kinds of biochar could be attributed to differences in properties of biochar with at least 95% confidence.

## 5.0 Results and Discussion

### 5.1 Sulfur XANES Analyses of Functionalized Biochar

Although Sulfur K-edge XANES spectra were collected on a large number of standards, only cysteine, sulfide, and sulfate standards are analyzed here with respect to doped biochar. Energies of the absorption edges increase in the order sulfide < cysteine < biochar < sulfate (arrow 1, **Fig. 12**).

Cysteine and biochar exhibit higher and narrower white lines than sulfide (arrow 2, **Fig. 12**). Moreover, the absorption edge of sulfate is offset by +8eV compared to biochar (arrow 3, **Fig. 12**) and the absorption edge of sulfide is offset by -2eV compared to doped biochar (arrow 4, **Fig. 12**). Thus, cysteine was the primary sulfur species functionalized to the SH-doped biochars.

### 5.2 Zinc XANES Analyses of Functionalized Biochar

Zinc K-edge XANES spectra for zinc sulfide (ZnS) complexes, zinc oxide (ZnO) complexes, and ZnO-doped RHB display significant spectral features. Energy of the absorption edges increase in the order ZnS < biochar < ZnO (arrow 1, **Fig. 13**).

ZnO and biochar exhibit much higher white lines than ZnS complexes (arrow 2, **Fig. 13**) and have oscillatory features at 9690eV, which are missing for ZnS complexes (arrow 3, **Fig. 13**).

Furthermore, ZnS shows a more pronounced shoulder at 9680eV compared to either ZnO or biochar (arrow 4, **Fig. 13**). Hence, it can be concluded that ZnO was the predominant zinc species functionalized to ZnO-doped biochar.

### 5.3 Manganese XANES Analyses of Functionalized Biochar

Comparing standard manganese-(II) oxide (MnO) and pyrolusite manganese-(IV) oxide ( $\beta$ -MnO<sub>2</sub>) K-edge XANES spectra to MnO<sub>2</sub>-doped RHB manganese XANES spectra, absorption edge energies increase in the order MnO < biochar <  $\beta$ -MnO<sub>2</sub> (arrow 1, **Fig. 14**).  $\beta$ -MnO<sub>2</sub> and biochar white lines are much broader and smaller compared to MnO complexes (arrow 2, **Fig. 14**). The energy of the peak for the sample is well aligned with the Mn(IV)-oxide.

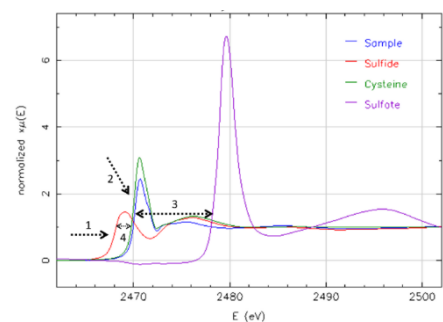


**Figure 12** XANES of SH doped RBH. (Image acquired from: Argonne National Lab Lemont, IL)

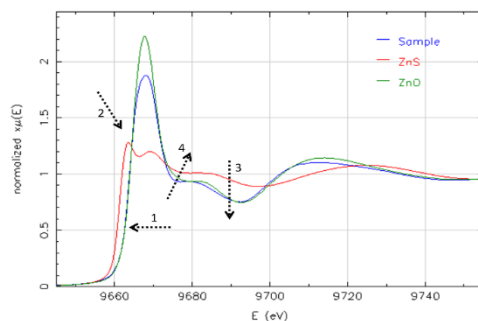


**Figure 13** XANES of ZnO-SH doped RBH. (Image acquired from: Argonne National Lab Lemont, IL)

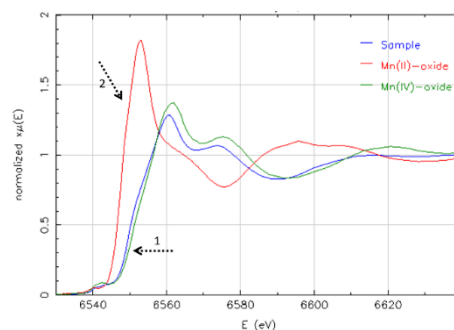


**Figure 14** XANES of MnO<sub>2</sub>-SH doped RBH. (Image acquired from: Argonne National Lab Lemont, IL)

Therefore,  $\beta$ - $\text{MnO}_2$  (pyrolusite) was the primary manganese species functionalized to the  $\text{MnO}_2$ -doped biochars. XANES Spectra for  $\text{MnO}_2$ -SH doped milled RHB,  $\text{MnO}_2$ -SH doped unmilled RHB, ZnO-SH doped RHB, and SH doped RHB all demonstrated that functionalization was successful. Since dopants were successfully added to the biochar, comparisons between properties of different types of biochar are valid.

## 5.4 Removal of Pesticides from Water

### 5.4.1 Data and Results

The data shows that  $\text{MnO}_2$ -SH doped milled RHB was the most effective for pp-DDT and pp-DDE removal from water (Table 1).

Biochar Type	pp-DDT	pp-DDE
$\text{MnO}_2$ -SH doped rice husk milled	98.31%	94.57%
$\text{MnO}_2$ -SH doped rice husk	85.77%	81.77%
ZnO-SH doped rice husk	74.45%	79.72%
SH doped rice husk	80.58%	76.92%
Undoped rice husk	78.75%	74.90%
Undoped oak wood	89.82%	90.05%

**Table 1** Percent of pesticides and emerging contaminants removed from water.

### 5.4.2 Statistical Significance

Additionally, all data groups were significantly different from each other at 97% or higher confidence levels (Table 2). Thus, all variations in data were due to differences in properties of biochars.

	$\text{MnO}_2$ -SH milled rice husk	$\text{MnO}_2$ -SH rice husk	ZnO-SH rice husk	SH rice husk	Undoped rice husk	Undoped oak wood
$\text{MnO}_2$ -SH milled rice husk		Confidence: 99%	Confidence: 99%	Confidence: 99%	Confidence: 99%	Confidence: 98%
$\text{MnO}_2$ -SH rice husk	Confidence: 99%		Confidence: 99%	Confidence: 99%	Confidence: 99%	Confidence: 95%
ZnO-SH rice husk	Confidence: 99%	Confidence: 99%		Confidence: 99%	Confidence: 99%	Confidence: 99%
SH rice husk	Confidence: 99%	Confidence: 99%	Confidence: 99%		Confidence: 97%	Confidence: 99%
Undoped rice husk	Confidence: 99%	Confidence: 99%	Confidence: 99%	Confidence: 97%		Confidence: 99%
Undoped oak wood	Confidence: 98%	Confidence: 95%	Confidence: 99%	Confidence: 99%	Confidence: 99%	

**Table 2** Confidence levels for significance tests (2-sample t-tests) between data from Table 1 for pp-DDT.

### 5.4.3 Observations and Discussion

According to Table 1, the percentage of pp-DDT removed for  $\text{MnO}_2$ -SH doped milled RHB was 12.54% higher as compared to  $\text{MnO}_2$ -SH doped RHB. This vast difference between milled and unmilled biochar sequestration efficiency can be explained by surface area – the higher surface area of the milled biochar allowed more reactions for contaminant sequestration.

The percentage of pp-DDT removed for  $\text{MnO}_2$ -SH doped RHB was 5.19% higher as compared to SH doped RHB. Thus, catalyst ( $\text{MnO}_2$ ) presence led to increased contaminant sequestration.

ZnO-SH doped RHB removed 6.13% less pp-DDT than SH-doped RHB. ZnO homogenized macropores of the biochar and decreased the average micro-pore size; hence, decreased micropore size actually led to decreased contaminant sequestration. This may be because hydrophobic organochlorines are known to form large aggregate complexes in aqueous solutions and smaller pores are better suited for mechanical trapping of these aggregates.

1.83% more pp-DDT was removed by SH doped rice husk biochar as compared to undoped rice husk biochar (**Table 1**). Thus, dopant (SH) presence led to increased contaminant sequestration, but did not contribute significantly to contaminant removal. However, there is also a significant difference of 7.03% between the pp-DDT removal efficiency of MnO<sub>2</sub>-SH doped unmilled RHB and undoped RHB (**Table 1**). This indicates that the sequestration mechanism for pp-DDT and pp-DDE was de-chlorination of the peripheral chlorines (**Fig. 15a**).

#### 5.4.4 Proposed Reaction Mechanism

The C-Cl bond energy in pp-DDT is 177kJ/mol. De-chlorination and subsequent binding to the thiol group yields a C-S bond, which has a bond energy of 272kJ/mol. Since the reactions which form stronger bonds tend to occur spontaneously, this reaction is spontaneous. Furthermore, MnO<sub>2</sub> is a known catalyst and can hence lower the activation energy for the reaction, allowing the pp-DDT to be sequestered from the contaminated water. This may also account for the relatively lower removal rates for pp-DDE (~5% less for both MnO<sub>2</sub>-SH doped milled RHB and MnO<sub>2</sub>-SH doped unmilled RHB). Since pp-DDE has 1 less chlorine atom than pp-DDT (**Fig. 15b** and **Fig. 15c**), this reaction was less likely to occur, and hence a smaller percentage of the pp-DDE was removed.

Thus, MnO<sub>2</sub>-SH doping can also be used to remove other toxic pesticides with peripheral chlorines such as heptachlor and dieldrin (**Fig. 15d** and **15e**).

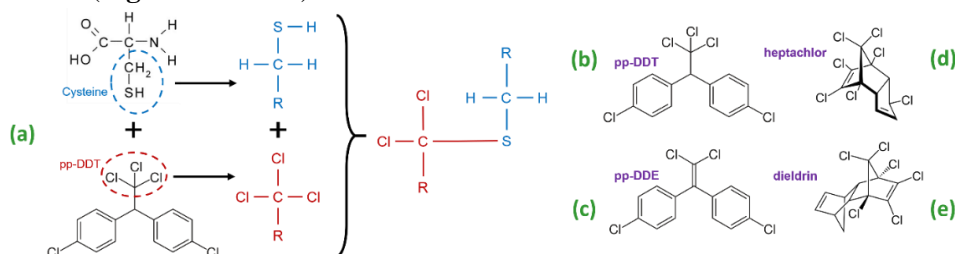


**Fig. 15** (a) Proposed mechanism for de-chlorination of pp-DDT and sequestration; (b) structure of pp-DDT; (c) structure of pp-DDE; (d) structure of heptachlor; (e) structure of dieldrin.

(Image created by: Eshani Jha)

## 5.5 Removal of Pharmaceuticals from Water

### 5.5.1 Data and Results

The data shows that the SH-functionalized, MnO<sub>2</sub>-doped milled RHB was the most effective for dimetridazole removal as well (**Table 3**).

Biochar Type	Dimetridazole
MnO <sub>2</sub> -SH doped rice husk milled	53.34%
MnO <sub>2</sub> -SH doped rice husk	29.18%
ZnO-SH doped rice husk	44.48%
SH doped rice husk	15.29%
Undoped rice husk	-1.55%
Undoped oak wood	20.45%

**Table 3** Percent of pesticides and emerging contaminants removed from water.

### 5.5.2 Statistical Significance

All data groups were significantly different from each other at 99% or higher confidence levels (**Table 4**). Thus, all variations in data were due to differences in properties of biochars.

	MnO <sub>2</sub> -SH milled rice husk	MnO <sub>2</sub> -SH rice husk	ZnO-SH rice husk	SH rice husk	Undoped rice husk	Undoped oak wood

MnO <sub>2</sub> -SH milled rice husk		Confidence: 99%				
MnO <sub>2</sub> -SH rice husk	Confidence: 99%		Confidence: 99%	Confidence: 99%	Confidence: 99%	Confidence: 99%
ZnO-SH rice husk	Confidence: 99%	Confidence: 99%		Confidence: 99%	Confidence: 99%	Confidence: 99%
SH rice husk	Confidence: 99%	Confidence: 99%	Confidence: 99%		Confidence: 99%	Confidence: 99%
Undoped rice husk	Confidence: 99%	Confidence: 99%	Confidence: 99%	Confidence: 99%		Confidence: 99%
Undoped oak wood	Confidence: 99%					

**Table 4** Confidence levels for significance tests (2-sample t-tests) between data from **Table 3** for dimetridazole.

### 5.5.3 Observations and Discussion

In general, the data obtained for dimetridazole reflects the same trends as pp-DDT and pp-DDE. But although MnO<sub>2</sub>-SH doped milled RHB was most effective for dimetridazole removal at 53.34%, ZnO doping (and hence decreased pore size) had the most dramatic impact on contaminant removal: ZnO-SH doped RHB removed 29.29% more dimetridazole than SH-doped RHB at 44.48% while MnO<sub>2</sub>-SH doped RHB only removed only 13.89% more at 29.18%.

The results obtained for undoped RHB require further explanation. From **Table 3**, it can be seen that an average of -1.55% of dimetridazole was removed. There are two possible explanations for this. The first explanation is that dimetridazole was preexistent in the biochar itself. However, the initial RHB matrix solutions (effluent from the biochar prewash) did not contain any traces of dimetridazole. Hence, it was not preexistent in the biochar. Alternatively, the actual percent of dimetridazole removed may be ~0%. Then, the negative reading is due to the error of the GC-MS machine. Since 1.55% falls beneath the error bar of 2% obtained from the standard deviation of the data, all data groups are still significantly different from each other, as shown in **Table 4**.

### 5.5.4 Proposed Reaction Mechanism

All parameters (i.e. surface area, catalytic properties, pore size, surface complexing agents, and carbon composition) impacted contaminant removal by more than 10%, the structure of dimetridazole (**Fig. 16**) suggests that functional groups are key to dimetridazole sequestration. Because dimetridazole has both a partial positive and a partial negative charge (**Fig. 16a**), polar functional groups (e.g. hydroxyl groups, **Fig. 16b**, or carboxyl groups, **Fig. 16c**) may play a significant role in contaminant removal.

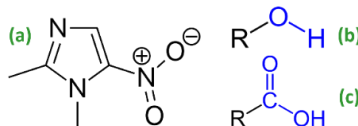


**Fig. 16** (a) Structure of dimetridazole; (b) hydroxyl functional group; (c) carboxyl functional group.  
(Image created by: Eshani Jha)

## 5.6 Removal of Microplastics from Water

### 5.6.1 Data and Results

The data shows that the ZnO-SH doped RHB was the most effective for BPA removal (**Table 5**).

Biochar Type	BPA
MnO <sub>2</sub> -SH doped rice husk milled	95.96%
MnO <sub>2</sub> -SH doped rice husk	93.12%
ZnO-SH doped rice husk	96.49%
SH doped rice husk	92.54%

Undoped rice husk	83.08%
Undoped oak wood	80.64%

**Table 5** Percent of pesticides and emerging contaminants removed from water.

### 5.6.2 Statistical Significance

All data groups for BPA removal were significantly different from each other at 98% or higher confidence levels (**Table 6**). Thus, all variations in data were due to differences in properties of biochars.

	MnO <sub>2</sub> -SH milled rice husk	MnO <sub>2</sub> -SH rice husk	ZnO-SH rice husk	SH rice husk	Undoped rice husk	Undoped oak wood
MnO <sub>2</sub> -SH milled rice husk		Confidence: 98%	Confidence: 99%	Confidence: 99%	Confidence: 99%	Confidence: 99%
MnO <sub>2</sub> -SH rice husk	Confidence: 98%		Confidence: 98%	Confidence: 99%	Confidence: 99%	Confidence: 99%
ZnO-SH rice husk	Confidence: 99%	Confidence: 98%		Confidence: 99%	Confidence: 99%	Confidence: 99%
SH rice husk	Confidence: 99%	Confidence: 99%	Confidence: 99%		Confidence: 99%	Confidence: 99%
Undoped rice husk	Confidence: 99%	Confidence: 99%	Confidence: 99%	Confidence: 99%		Confidence: 99%
Undoped oak wood	Confidence: 99%	Confidence: 99%	Confidence: 99%	Confidence: 99%	Confidence: 99%	

**Table 6** Confidence levels for significance tests (2-sample t-tests) between data from **Table 1** for BPA.

### 5.6.3 Observations and Discussion

Although the data reflects trends similar to those obtained for organochlorines, ZnO-SH doped RHB was most effective for BPA removal at 96.49% removed. However, thiol presence had the greatest impact on removal efficiency at 8.56% more removed by SH-doped RHB compared to undoped RHB. In comparison, surface area, catalyst presence, pore size, and carbon composition impacted BPA sequestration by less than 5% impact on contaminant removal.

### 5.6.4 Proposed Reaction Mechanism

Since thiol presence had greatest effect on BPA removal, the sequestration mechanism likely involves adsorption of BPA by thiols. Since BPA is a planar molecule composed of carbon rings, carbon  $\pi$  bonds form electron cloud rings above and below the plane of the molecule (**Fig. 17a**). These  $\pi$  electron clouds of the aromatic rings may interact with the lone pair electron cloud of the sulfur atom in SH (**Fig. 17b**). This SH- $\pi$  interaction between BPA and SH is probably the driving removal mechanism.

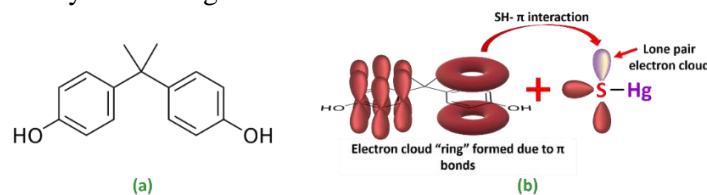


**Fig. 17** (a) Structure of BPA; (b) Proposed mechanism for SH- $\pi$  interactions and BPA sequestration.

(Image created by: Eshani Jha)

## 5.7 Removal of Heavy Metals from Water

### 5.7.1 Data and Results

The data shows that MnO<sub>2</sub>-SH doped milled RHB was most effective for heavy metal removal (**Table 7**).

Biochar Type	Arsenic	Lead	Mercury	Cadmium
--------------	---------	------	---------	---------

MnO <sub>2</sub> -SH doped rice husk milled	97.78%	98.23%	100.00%	100.00%
MnO <sub>2</sub> -SH doped rice husk	96.39%	95.39%	97.12%	98.79%
ZnO-SH doped rice husk	94.99%	95.60%	99.66%	100.00%
SH doped rice husk	95.10%	97.46%	98.14%	99.33%
Undoped rice husk	46.48%	65.28%	64.30%	48.81%
Undoped oak wood	52.25%	68.38%	69.92%	55.68%

**Table 7** Percent of heavy metals removed from water.

### 5.7.2 Statistical Significance

Most data groups for heavy metal removal were significantly different from each other at 97% or higher confidence levels (**Table 8**, averages across all heavy metals). Thus, most variations in data were due to differences in properties of biochars.

	MnO <sub>2</sub> -SH milled rice husk	MnO <sub>2</sub> -SH rice husk	ZnO-SH rice husk	SH rice husk	Undoped rice husk	Undoped oak wood
MnO <sub>2</sub> -SH milled rice husk		Confidence: 99%	Confidence: 99%	Confidence: 99%	Confidence: 99%	Confidence: 98%
MnO <sub>2</sub> -SH rice husk	Confidence: 99%		Confidence: 20%	Confidence: 20%	Confidence: 99%	Confidence: 95%
ZnO-SH rice husk	Confidence: 99%	Confidence: 20%		Confidence: 15%	Confidence: 99%	Confidence: 99%
SH rice husk	Confidence: 99%	Confidence: 20%	Confidence: 15%		Confidence: 97%	Confidence: 97%
Undoped rice husk	Confidence: 99%	Confidence: 99%	Confidence: 99%	Confidence: 97%		Confidence: 99%
Undoped oak wood	Confidence: 98%	Confidence: 95%	Confidence: 99%	Confidence: 99%	Confidence: 99%	

**Table 8** Confidence levels for significance tests (2-sample t-tests) between data from **Table 5**, averaged across all heavy metals.

### 5.7.3 Observations and Discussion

According to **Table 8**, there was no statistical difference between MnO<sub>2</sub>-SH doped rice husk biochar, ZnO-SH doped rice husk biochar, or SH-doped rice husk biochar. Thus, catalyst presence and pore size have no appreciable effect of contaminant removal. However, higher surface area, dopant presence, and increased carbon composition all contributed to increased adsorption.

At the concentration tested (100µM), the percent of arsenic removed averaged less than percent lead, mercury, or cadmium removed (**Table 7**). This may be due to arsenic's chemical properties. In water, arsenic mainly exists in 2 inorganic forms: arsenite and arsenate. Arsenite is highly toxic. Arsenate is much less toxic, but arsenate analyses by ICP-MS could have phosphate matrix effects. Since the initial feedstock for functionalized biochar production was rice husk, which is naturally rich in phosphates, there could have been an overstatement of arsenic concentration in the filtered water due to the matrix effect coming from spectrum interference with phosphates. Most likely, the remaining concentration of arsenic is about 2% less than reported.

Some loss of heavy metals was observed in the solutions used for ICP-MS calibration due to sorption of contaminants to reactors. This error is small enough to fall under the error bar of ± 2% for arsenic, lead, and cadmium. In mercury, however, this loss did not fall under the ± 2% error bar, reaching up to 5.63% in the most extreme case. This is due to mercury's "stickiness," which causes it to easily sorb to reactor vessels, resulting in mass balance issues. This is, in fact, a well-known problem for analytical chemists as mercury residues are found in equipment long after experiments (sometimes several months). Mercury residues are likely to be found when mercury is adsorbed to a matrix (e.g. glass). This is likely the reason why mercury concentrations decreased so dramatically in the controls.

### 5.7.4 Proposed Reaction Mechanism

Thiol functionalization had the most dramatic impact on performance with a 40.83% average increase in percent removed across all heavy metals (**Table 7**). This indicates that the sequestration mechanism was likely dependent on thiol-contaminant interactions (**Fig. 18**).

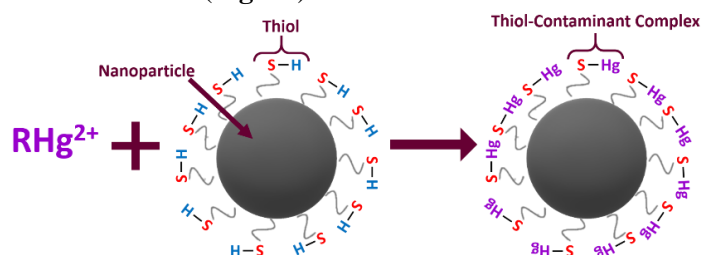


**Fig. 18** Proposed mechanism for heavy metal removal from water. Here,  $\text{RHg}^{2+}$  represents the mercury ion, but this may be replaced with any other ion (e.g.  $\text{Pb}^{2+}$  for lead).

(Image created by: Eshani Jha)

## 6.0 Engineering Application

One application of functionalized biochar is for remediation of drinking water. This is especially important in regions that use recycled wastewater (e.g. Orange County, CA and Singapore), groundwater (e.g. agricultural areas US), and older pipelines (e.g. Flint, MI and San Francisco, CA).

### 6.1 Prior Art and Market Analysis

Current advanced water filters designed by universities (e.g. UC Berkeley, Old Dominion, and UI Chicago) are designed to target only one or two heavy metal contaminants (**Table 9**). They do not address organic contamination and have extraordinarily slow flow rates. Current water filters on the market (e.g. Travel Berkey) target inorganic and organic contaminants (**Table 9**). However, they remove only 90% of contaminants present. They also have exorbitant prices (e.g. \$249 for a tabletop filter), which makes them inaccessible for the majority of people in dire need of these filters.

	Contaminant	UC Berkeley	Old Dominion	UI Chicago	Travel Berkey
% Contaminants Removed	Arsenic	99	NA	NA	90
	Lead	NA	80	75	90
	Mercury	NA	NA	NA	90
	Cadmium	NA	NA	18	90
	pp-DDT	NA	NA	NA	NA
	pp-DDE	NA	NA	NA	NA
	BPA	NA	NA	NA	NA
	Dimetridazole	NA	NA	NA	NA
Other	Flow rate	0.17L/min	0.30L/min	0.66L/min	0.17L/min
	Cost	\$15/year	NA	NA	\$249

**Table 9** Effectiveness of current water filters.

### 6.2 Design and Simulation

The goal of the next stage of this research is to create a highly efficient, sustainable, and affordable water purification system for the rapid removal of organic and inorganic contaminants from water (filter design in **Fig. 19-22**). Simulations have shown the expected flow rate to be 1L/min.

The first compartment is designed to hold contaminated water for filtration (**Fig. 20**).

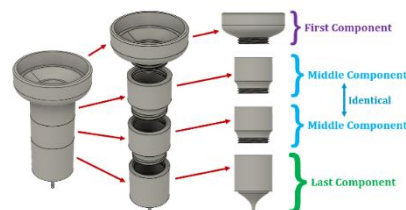


**Fig. 19** Full view of filter.

(Image created by: Eshani Jha)

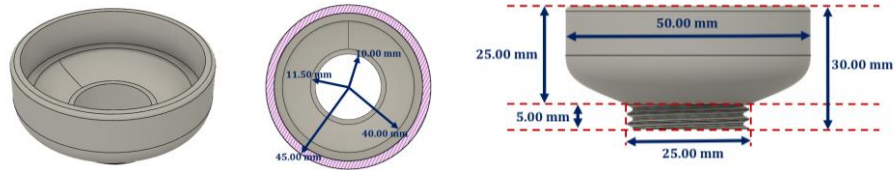


**Fig. 20** View of first component (*Left*), top view of cross section of component (*Middle*), right view of component (*Right*).  
(Image created by: Eshani Jha)

The first middle compartment is designed to hold sand (silica, SiO<sub>2</sub>) (**Fig. 21**). Silica is known to trap particles and remove viruses. By removing larger contaminants, this layer helps prevent clogging of biochar micropores. Silica is held with filter paper with pore size 500µm. The second middle compartment is designed to hold calcite (CaCO<sub>3</sub>) (**Fig. 21**). Calcite enhances clumping of granular materials. However, since it can cause water to become hard, stearic acid (a kind of fatty acid) will be coated onto the calcite. This layer also removes large particles and contaminants. Calcite is held with filter paper with pore size 200µm.

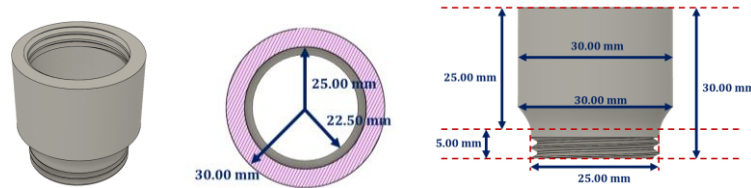


**Fig. 21** View of last component (*Left*), top view of cross section of component (*Middle*), right view of component (*Right*).  
(Image created by: Eshani Jha)

The last component is design to hold functionalized biochar (**Fig. 22**). Filter paper with pore size 65µm is used to hold the biochar.

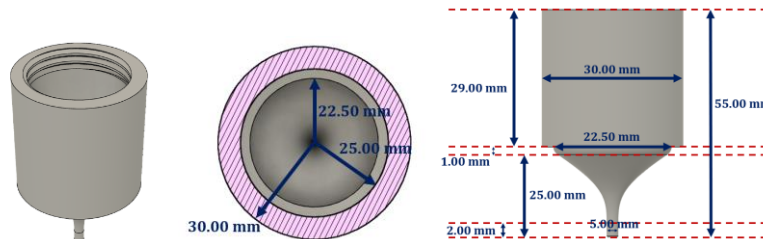


**Fig. 22** View of last component (*Left*), top view of cross section of component (*Middle*), right view of component (*Right*).  
(Image created by: Eshani Jha)

The average family needs:

$$\frac{2L \text{ water}}{\text{person every day}} \times \frac{4 \text{ people}}{\text{household}} \times \frac{30 \text{ days}}{\text{month}} = 240L \text{ drinking water/month}$$

Since 0.5g of biochar is expected to filter up to 5,000L of water, one replacement should last:

$$\frac{5000 \text{ L}}{240 \text{ L/month}} = 20.8 \text{ months} \approx 20 \text{ months}$$

This corresponds to:

$$\frac{0.5g \text{ biochar}}{20 \text{ months}} \times \frac{\$40.00}{g \text{ of biochar}} = \$1.00/\text{month}$$

Thus, the floating cost (cost of functionalized biochar replacement) will be \$1.00/month and the one-time cost is expected to be \$15.00 (cost of plastic and functionalized biochar).

Mass production will lower both of these costs at least 5 times. Hence, the one-time cost will be under \$3 and the floating cost will be under 20 cents per month.

### 6.3 Prototype Testing

A 3-D printed prototype of the design (**Fig. 23**) was printed using polycarbonate printing material. Sand, calcite, and biochar were placed in respective compartments (total 0.5g sand, calcite, and biochar). Tap water was passed through the filter for 10 minutes. This was repeated 3 times. The flow rate was determined to be 1.03 L/min, which is consistent with the simulation prediction of 1.0 L/min (**Fig. 23**).

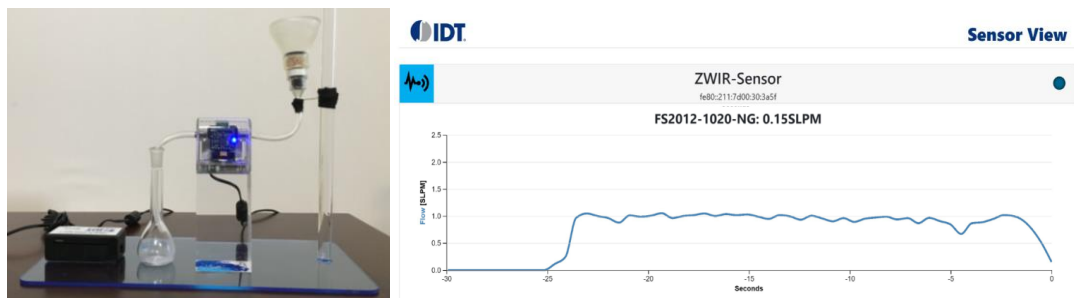


**Fig. 23** The prototype designed to mimic the structure of a commercial filter ( $L$ ) had an average flow rate of 1.03L/min ( $R$ ) with a floating cost of \$1/month.

(Picture taken by: Eshani Jha)

## 6.4 Testing of Manufactured Filter

I have submitted my prototype and design to Greenfield Labs of Ford Motor Company to manufacture and test my filter on industrial waste water. Production and testing are in progress.

## 7.0 Conclusion and Expected Impact

### 7.1 Summary

1. Milled rice husk biochar functionalized with  $MnO_2$  and SH effectively removed over 98% pp-DDT, 94% pp-DDE, 53% dimetridazole, 95% BPA, 95% arsenic, 98% lead, and 100% mercury and cadmium for initial contaminant concentrations of  $100\mu M$ .
2. This material was significantly more effective than the other five types of biochar tested, including unmilled  $MnO_2$  and SH doped biochar at the 99.99% confidence level.
3. Oak wood biochar was at least 10% more effective than rice husk biochar due to its large carbon composition and pore volume.
4. General trends in data demonstrate that high surface area, catalyst presence, increased pore size, thiol doping, and high carbon composition are key for contaminant sequestration.
5. The prototype for drinking water filtration had a flow rate of 1.03 L/min, which exceeds that of commercial and university-developed filters.
6. The one-time cost is expected to be \$3 (cost of plastic and functionalized biochar) and floating cost is expected to be 20 cents (cost of functionalized biochar replacement).

### 7.2 Expected Impact

These results clearly suggest that functionalized biochars have the potential to revolutionize the water filtration industry. Not only is functionalized biochar production inexpensive, but it is also extremely safe and effective. Also, the initial feedstock for biochar production can be a biogenic waste (e.g. rice husk) leading to a truly circular economy in which a waste feedstock is used as a resource for water filtration. Choice of waste feedstocks for synthesizing biochar used for water filtration devices also makes it a highly affordable and sustainable. However, additional testing will be required for biochars synthesized from other feedstocks.

### 7.3 Additional Future Work

The scope of water purification by biochar can be expanded to pathogens and bacteria through functionalization of silver nanoparticles onto biochar. Silver has an oligodynamic effect and is toxic for bacteria, algae, and fungi [34]. Furthermore, it is incorporated by bacteria it kills. Hence, dead bacteria may kill additional bacteria by acting as a source for silver [35]. Silver generally has low toxicity, and minimal risk is expected when silver is used in trace quantities [34].

## 8.0 References

1. 2.1 billion people lack safe drinking water at home, more than twice as many lack safe sanitation. (n.d.). Retrieved from <https://www.who.int/news-room/detail/12-07-2017-2-1-billion-people-lack-safe-drinking-water-at-home-more-than-twice-as-many-lack-safe-sanitation>.
2. Denchak, M. (2019, November 13). Water Pollution: Everything You Need to Know. Retrieved from <https://www.nrdc.org/stories/water-pollution-everything-you-need-know>.
3. Information on Earth's water. (n.d.). Retrieved from <https://www.ngwa.org/what-is-groundwater/About-groundwater/information-on-earths-water>.
4. Substance Priority List. (2017, August 10). Retrieved from <https://www.atsdr.cdc.gov/spl/>.
5. Pesticide residues in food. (n.d.). Retrieved from <https://www.who.int/news-room/fact-sheets/detail/pesticide-residues-in-food>.
6. Jayaraj, R., Megha, P., & Sreedev, P. (2016). Organochlorine pesticides, their toxic effects on living organisms and their fate in the environment. *Interdiscip Toxicol* 9 (3–4): 90–100.
7. *Toxicology Profile for 4,4'-DDT, 4,4'-DDE, 4,4'-DDD (Update)*; U. S. Department of Human Health & Human Services, Agency for Toxic Substances and Disease Registry, 1994.
8. Chattopadhyay, S., & Chattopadhyay, D. (2015). Remediation of DDT and its metabolites in contaminated sediment. *Current Pollution Reports*, 1(4), 248-264.
9. "Contaminants of Emerging Concern in the Environment". *Environmental Health—Toxic Substances Hydrology Program*. Reston, VA: U.S. Geological Survey. 2017-06-16.
10. Martin, M. J., Thottathil, S. E., & Newman, T. B. (2015). Antibiotics overuse in animal agriculture: a call to action for health care providers.
11. Zhang, X., Li, Y., Liu, B., Wang, J., Feng, C., Gao, M., & Wang, L. (2014). Prevalence of veterinary antibiotics and antibiotic-resistant *Escherichia coli* in the surface water of a livestock production region in northern China. *PLoS One*, 9(11).
12. Ventola, C. L. (2015). The antibiotic resistance crisis: part 1: causes and threats. *Pharmacy and therapeutics*, 40(4), 277.
13. Carwile, J. L., Ye, X., Zhou, X., Calafat, A. M., & Michels, K. B. (2011). Canned soup consumption and urinary bisphenol A: a randomized crossover trial. *Jama*, 306(20), 2218-2220.
14. Geens, T., Apelbaum, T. Z., Goeyens, L., Neels, H., & Covaci, A. (2010). Intake of bisphenol A from canned beverages and foods on the Belgian market. *Food Additives and Contaminants*, 27(11), 1627-1637.
15. Superfund: National Priorities List (NPL). (2018, June 4). Retrieved from <https://www.epa.gov/superfund/superfund-national-priorities-list-npl>.
16. Masindi, V., & Muedi, K. L. (2018). Environmental contamination by heavy metals. *Heavy Metals*, 19, 2019.
17. Lanphear, B. P., Rauch, S., Auinger, P., Allen, R. W., & Hornung, R. W. (2018). Low-level lead exposure and mortality in US adults: a population-based cohort study. *The Lancet Public Health*, 3(4), e177-e184.
18. Gould, E. (2009). Childhood lead poisoning: conservative estimates of the social and economic benefits of lead hazard control. *Environmental health perspectives*, 117(7), 1162-1167.
19. Ross, H., & Mannion, G. (2012). Curriculum making as the enactment of dwelling in places. *Studies in Philosophy and Education*, 31(3), 303-313.
20. Gaffney, J. S., & Marley, N. (2014). In-depth review of atmospheric mercury: sources, transformations, and potential sinks. *Energy and Emission Control Technologies*, 2, 1-21.
21. Wilson, D. N. (1988). Cadmium-market trends and influences. In *Cadmium 87. Proceedings of the 6th International Cadmium Conference, London, Cadmium Association* (Vol. 9, p. 16).
22. Faroon, O., Ashizawa, A., Wright, S., Tucker, P., Jenkins, K., Ingerman, L., & Rudisill, C. (2012). Toxicological profile for cadmium.
23. Suffet, I. H. (1980). An evaluation of activated carbon for drinking water treatment: National Academy of Science report. *Journal-American Water Works Association*, 72(1), 41-50.
24. Manyà, J. J. (2012). Pyrolysis for biochar purposes: a review to establish current knowledge gaps and research needs. *Environmental science & technology*, 46(15), 7939-7954.
25. Gai, X., Wang, H., Liu, J., Zhai, L., Liu, S., Ren, T., & Liu, H. (2014). Effects of feedstock and pyrolysis temperature on biochar adsorption of ammonium and nitrate. *PloS one*, 9(12).
26. Liu, Z., Quek, A., Hoekman, S. K., & Balasubramanian, R. (2013). Production of solid biochar fuel from waste biomass by hydrothermal carbonization. *Fuel*, 103, 943-949.
27. Genovese, M., Jiang, J., Lian, K., & Holm, N. (2015). High capacitive performance of exfoliated biochar nanosheets from biomass waste corn cob. *Journal of Materials Chemistry A*, 3(6), 2903-2913.

28. Liu, W. J., Jiang, H., & Yu, H. Q. (2015). Development of biochar-based functional materials: toward a sustainable platform carbon material. *Chemical reviews*, 115(22), 12251-12285.
29. Deliyanni, E., Bandosz, T. J., & Matis, K. A. (2013). Impregnation of activated carbon by iron oxyhydroxide and its effect on arsenate removal. *Journal of Chemical Technology & Biotechnology*, 88(6), 1058-1066.
30. Tebo, B. M., Bargar, J. R., Clement, B. G., Dick, G. J., Murray, K. J., Parker, D., ... & Webb, S. M. (2004). Biogenic manganese oxides: properties and mechanisms of formation. *Annu. Rev. Earth Planet. Sci.*, 32, 287-328.
31. Dick, G. J. (2006). *Microbial manganese (II) oxidation: biogeochemistry of a deep-sea hydrothermal plume, enzymatic mechanism, and genomic perspectives* (Doctoral dissertation, UC San Diego).
32. Brewer, C. E. (2012). Biochar characterization and engineering.
33. Speight, J. G. (2016). *Environmental organic chemistry for engineers*. Butterworth-Heinemann.
34. Lansdown, A. B. (2006). Silver in health care: antimicrobial effects and safety in use. In *Biofunctional textiles and the skin* (Vol. 33, pp. 17-34). Karger Publishers.
35. Wakshlak, R. B. K., Pedahzur, R., & Avnir, D. (2015). Antibacterial activity of silver-killed bacteria: the "zombies" effect. *Scientific reports*, 5, 9555.